Physics of Plasmas ARTICLE scitation.org/journal/php

Loss of bootstrap current in vicinity of magnetic islands

Cite as: Phys. Plasmas **26**, 052516 (2019); doi: 10.1063/1.5084300
Submitted: 6 December 2018 · Accepted: 3 May 2019 ·
Published Online: 23 May 2019

Feng Wang,[1] Jiquan Li,[1,a)] Hongpeng Qu,[1] Xiaodong Peng,[1] and Yong Xiao[2]

AFFILIATIONS

[1]Southwestern Institute of Physics, Chengdu, Sichuan 610041, People's Republic of China
[2]Zhejiang University, Hangzhou, Zhejiang 310058, People's Republic of China

[a)]Author to whom correspondence should be addressed: lijq@swip.ac.cn

ABSTRACT

Profiles of the ion density and bootstrap current in the vicinity of magnetic islands are investigated based on the first principles gyro-kinetic particle simulation via the gyro-kinetic toroidal code. The physics on the recovery of the ion density gradient inside the islands in various collision regimes is discussed. Simulation results show that for small magnetic islands, the ion density gradient can survive inside the island due to the combination effect of both the banana-orbit width of trapped ions and the drift-orbit displacement of passing ions. It is suggested that the recovery of the pressure gradient inside small islands may play a more important role in the reduction of driving force of the ion bootstrap current in the evolution of the neoclassical tearing mode, rather than the so-called finite banana-orbit effects.

I. INTRODUCTION

Plasmas can be confined in a fusion device, for instance, a tokamak, because charged particles move mainly along the magnetic field lines on the nested flux surfaces. However, magnetic islands, which can be generated by MHD activities such as tearing modes, may lead to the reduction of the plasma confinement. Usually, the evolution of the tearing instability is governed by the perturbed parallel current density in the vicinity of islands. The current perturbation results from various sources such as the bootstrap current, which have been introduced to explain the observations on the tearing instabilities in the tokamak experiment.[1–5] The early study of the classical tearing instability has only considered the inductive current. However, due to the toroidal configuration of the tokamak plasma, the fast movement of charged particles along the perturbed magnetic field lines can flatten the radial pressure profile inside islands and thus result in a loss of the bootstrap current.[6,7] Such perturbation of the bootstrap current can provide an extra drive force for the island growth and hence destabilize the tearing modes. This instability corresponds to usually the so-called neoclassical tearing mode (NTM).[8,9]

Studies on understanding and controlling the NTMs are of crucial importance in present tokamak experiments since the NTMs can limit achievable pressure in tokamak plasmas. For this reason, the NTMs have been extensively investigated in the past few decades,[5,10–12] especially including the interaction between NTMs and turbulence transport.[13–16] Conventionally, it has been shown that the driving term of bootstrap current in the NTM evolution equation is inversely proportional to the island width. Such a relation indicates that all NTMs can grow to a saturation state from very small island seeds. However, the experimental observations show that there exists a threshold of magnetic island width for the NTM instability, suggesting that some stabilizing mechanisms may suppress the NTMs. Among the possible mechanisms, anomalous radial diffusion of the electrons near the island separatrix and the neoclassical polarization current originating from the time-dependent radial electric field in the vicinity of magnetic islands have been investigated for a long time.[2–4]

Besides, note that the bootstrap current contribution to NTM evolution is seeded by the responses of trapped particles to the radial pressure gradient. The early expressions of the bootstrap current term in the NTM evolution equation have been derived in the limit of large magnetic islands. Specifically, the island width is much larger than the finite-banana-width (FBW) of the trapped ion (i.e., $w \gg w_{ib}$, w is the magnetic island half-width, $w_{ib} = \varepsilon^{1/2}\rho_{i\theta}$ is the ion FBW, ε is the inverse aspect ratio, and $\rho_{i\theta}$ is the poloidal Larmor radius of thermal ions). However, the experimental observations have shown that the seed island width threshold of the NTMs is just comparable to the FBW of the thermal ion. In this situation, the conventional large island assumption and previous analytical expression of the ion bootstrap current contribution are unavailable in NTM research. Poli *et al.* have first used the "Monte-Carlo" method to investigate the ion density and bootstrap current distribution in the vicinity of islands.[10,17] In their

work, although the recovery of the ion density gradient inside small islands could be observed, it was also claimed that the survival of ion bootstrap current inside the small island and accordingly the drastic reduction of its contribution to NTM evolution are mainly due to the so-called FBW effect, i.e., the trapped ions inside the island can "feel" the pressure gradient outside the island. On the other hand, it has been shown that in our previous analytical work, the recovery of the ion pressure gradient may play an equal role at least as the FBW effect in the survival of the ion bootstrap current inside small islands.[18] Hornsby *et al.* have studied the density profile of trapped electrons with different diffusion coefficients due to turbulence via a simple model and found that a finite density gradient still exists inside the island when the diffusion is sufficiently strong.[19] In that work, the effect of the particle drift-orbit width has not been considered. Therefore, to further clarify the difference of the above results and identify the underlying physical mechanism, it is helpful to investigate the ion density and bootstrap current distribution in the vicinity of small islands more precisely by taking all the drift-orbit width effects into account. This is the main purpose of this work.

In the present work, we will discuss the ion density and bootstrap current profiles in the vicinity of the islands of the $(2,\ 1)$ tearing mode based on the first principles simulation through modifying gyro-kinetic toroidal code (GTC). Actually, GTC has long been adopted to investigate the density or current distribution in the vicinity of the island. Dong and Lin have demonstrated that the electron bootstrap current profile inside islands is related to the collisionality.[20] Jiang *et al.* have studied the effects of magnetic islands on drift wave instabilities.[21,22] Here, to compare with the results in Refs. 10 and 17, we focus our attention on the ion density and bootstrap current profiles inside the islands. The electron bootstrap current is not discussed in this work.

The remainder of this paper is organized as follows. The descriptions of magnetic island geometry and GTC are introduced in Sec. II. The equilibrium ion bootstrap current is investigated and compared with the analytical results as a benchmark. In Sec. III, we study the profiles of ion density and its gradient inside magnetic islands in various collision regimes. In Sec. IV, the profiles of ion bootstrap currents inside the islands with different widths in the banana regime are investigated. Finally, we summarize the main results in Sec. V.

II. NUMERICAL SCHEME OF GTC AND BENCHMARK

A. Island geometry

In this work, the equilibrium magnetic field can be written as

$$\vec{B}_0 = \delta\nabla\psi_p + I\nabla\theta + g\nabla\zeta = q\nabla\psi_p \times \nabla\theta - \nabla\psi_p \times \nabla\zeta.$$

Here, magnetic coordinates $(\psi_p,\ \theta,\ \zeta)$ have been adopted, where ψ_p is the poloidal flux and θ and ζ are the poloidal and toroidal angles, respectively. The Jacobian is $J = (gq + I)/B_0^2$, q is the safety factor, g and I are the poloidal and toroidal currents, respectively, and the radial component δ can be neglected in large aspect ratio tokamaks.

The tearing mode instability provides a perturbed radial magnetic field to generate magnetic islands, whose form is $\delta\vec{B} = \delta\tilde{B}\sin(m\theta - n\zeta)$. In this work, based on $\delta\vec{B} = \nabla \times \vec{A}_{||}$, the perturbed parallel vector potential can be described as

$$\delta\vec{A}_{||} = \frac{-r_s(R_0 + r_s)}{m(R_0 + r\cos\theta)}\delta\tilde{B}\cos(m\theta - n\zeta),$$

where m and n are the poloidal and toroidal mode numbers and R_0 is the major radius. The perturbed magnetic flux-surface of the islands can thus be expressed as

$$\Omega = \frac{2(\psi_p - \psi_{p,s})^2}{w^2} - \cos(m\theta - n\zeta),$$

where $w = 2\left(\psi_p q\delta\tilde{B}/\left(mB_0 dq/d\psi_p\right)\right)^{1/2}|_s$ is the half width of the island and the subscript "s" denotes that the physical quantity is evaluated at the rational surface where the magnetic islands are located. According to this definition, $\Omega = -1$ corresponds to the island center (O-point) and $\Omega = 1$ to the separatrix of a magnetic island. In our simulations, we keep at least 18 grids in the radial direction through the O-point inside the island.

B. Formulation and numerical scheme of GTC

GTC is a large-scale parallel computing code based on the first principles gyro-kinetic theory, which has been popularly utilized to investigate the instabilities, turbulence, and transport in tokamak plasmas. In this work, the profiles of particle density and bootstrap current in the vicinity of static magnetic islands with different widths are studied via GTC.

In GTC simulation, the dynamics of guiding centers are governed by the Hamiltonian in the phase space of $(\vec{X}, \mu, v_{||})$, where $\vec{X}$, μ, and $v_{||}$ denote the spatial coordinates, magnetic moment, and parallel velocity along the field line, respectively.

The accurate profile of ion bootstrap current can be achieved through solving the gyro-kinetic Vlasov equation

$$\frac{df}{dt} = \frac{\partial f}{\partial t} + \dot{\vec{X}}\cdot\nabla f + \dot{v}_{||}\frac{\partial f}{\partial v_{||}} - C(f) = 0, \tag{1}$$

$$\dot{\vec{X}} = v_{||}\frac{\vec{B}_0 + \delta\vec{B}}{\vec{B}_0} + \vec{v}_d, \tag{2}$$

where $\dot{v}_{||} = -\vec{B}^* \cdot \mu\nabla B_0/(m_i B_0)$, $\vec{v}_d = v_{||}{}^2\nabla\times\vec{b}_0/\Omega_i + \mu\vec{b}_0\times\nabla B_0/(m_i\Omega_i)$ is the magnetic drift velocity, $\vec{B}^* = \vec{B}_0^* + \delta\vec{B}$, $\vec{B}_0^* = \vec{B}_0 + B_0 v_{||}/\Omega_i\nabla\times(\vec{B}_0/B_0)$, Ω_i is the ion Larmor frequency, subscript "i" stands for the species of the ion, and $\delta\vec{B}$ is the magnetic field perturbation. A Fokker-Planck collision operator $C(f)$, which conserves the ion number, momentum, and energy, is adopted.[23] Only ion-ion collision is considered here because the ion mass is much larger than that of the electron.

A δf method is adopted in solving the gyro-kinetic Vlasov equation to reduce particle noise with a smaller number of particles compared to the full-f method.[24] The distribution function f in Eq. (1) can be separated into a time-independent equilibrium term f_0 and a time-evolving perturbed term δf. Equation (1) gives the first order equation

$$\frac{\partial\delta f}{\partial t} + \left(v_{||}\frac{\vec{B}_0}{B_0} + \vec{v}_d\right)\cdot\nabla\delta f + \dot{v}_{||}\frac{\partial\delta f}{\partial v_{||}} - C(\delta f) = \vec{v}_d\cdot\nabla f_0, \tag{3}$$

where f_0 is taken as a Maxwellian distribution for simplicity. The third term at the left hand side of Eq. (3) represents the effects of the banana

orbit of the trapped ion and orbit displacement of the passing ion. The weight equation derived from Eqs. (1)–(3) is

$$\frac{dw}{dt} = (1-w)\left(-v_{||}\frac{\delta\vec{B}}{B_0} + \vec{v}_d\right)\cdot\frac{\nabla f_0}{f_0}, \tag{4}$$

where $w = \delta f/f_0$ denotes the weight of markers in the simulation. This equation together with equations of particle motion, Eq. (2), can form a closed system for gyro-kinetic simulations of density and bootstrap current profiles in the presence of magnetic islands.

C. Benchmark of the numerical scheme

In this work, the radial profile of ion temperature is taken as uniform and only the density gradient is set as $n_i = n_0[1 + 0.205(\tanh((0.3 - \psi_p/\psi_w)/0.4) - 1)]$, where ψ_p and ψ_w are the poloidal magnetic flux and maximum poloidal magnetic flux, respectively. In our simulations, the major radius is taken as $R_0 = 83.5$ cm, the inverse aspect ratio is $a/R_0 = 0.3873$, a is the minor radius, and the magnetic field and ion temperature on the axis are $B_0 = 2T$ and $T_0 = 39$ ev, respectively. The safety factor profile is chosen as $q = 1.5 + 1.0\psi_p/\psi_w$. On the rational surface where $q = 2$, the half width of the ion banana orbit is taken as $w_b = q_s\rho_i/\sqrt{\varepsilon} = 4\rho_i$, the displacement of the passing ion orbit from the equilibrium flux-surface $w_p = q_s\rho_i = 2\rho_i$, $\kappa_n = 0.017\,\mathrm{cm}^{-1}$, and the effective ion-ion collisional frequency is defined as $\upsilon_{ii}^* = \varepsilon^{-1.5}\upsilon_{ii}\sqrt{2}qR_0/v_{th}$, where ρ_i is the ion Larmor orbit radius, ε is the local reverse aspect ratio, v_{th} is the thermal velocity, and υ_{ii} is the ion-ion collisional frequency.

To more conveniently explain simulation results in Secs. III and IV, it is helpful to simply recall the physical image of equilibrium ion bootstrap current. Ion bootstrap current in the tokamak plasmas can be generated by a combination of magnetic field inhomogeneity, pressure gradient, and collision. Due to the inhomogeneity of the tokamak magnetic field, some ions can be "trapped". If a radial density gradient of the trapped ion exists, a parallel flow of the trapped ions comes up on the magnetic surfaces.[25] Then, the passing ions can move with trapped ions via ion-ion collision, which produces the total ion bootstrap current. However, with the increase in collisional frequency, more and more trapped particles cannot perform a whole banana orbit before they come into a large-angle scattering and the ion bootstrap current decreases.[26] When collisional frequency becomes extremely high, the ion bootstrap current vanishes.

The bootstrap current in the limit of small collisional frequency is analytically expressed as $j_b = cf_tB_{p0}dp/dr$, where the fraction of trapped particles is $f_t = 1.46\sqrt{\varepsilon} - 0.46\varepsilon$.[27] Here, a GTC simulation on the radial profile of flux-surface-averaged ion bootstrap current in the case without islands is performed to verify our numerical scheme. Omitting the perturbed magnetic field in the equation of ion motion Eq. (2) and the weight equation of the ion, Eq. (4), the radial distribution of ion bootstrap current in the banana regime ($\upsilon_{ii}^* = 0.05$) is plotted in Fig. 1(a), where the current is normalized by n_0ev_{th}. The dependence of the bootstrap current (around the resonant surface of $q = 2$) on collisionality is plotted in Fig. 1(b). The results show that the bootstrap current decreases with the increase in collisional frequency.[26]

III. DENSITY PROFILE VS COLLISION FREQUENCY

In simulation, an island geometry with $(m, n) = (2, 1)$ is adopted and incorporated into the GTC code as introduced in Sec. II. The poloidal position of the O-points of two static islands is set at $\theta = 0$ and $\theta = \pi$, where the toroidal angle $\zeta = 0$. In other words, the two O-points are located at the low field side (LFS) and the high field side (HFS) of the tokamak magnetic configuration, respectively.

In this section, we will investigate the ion density profile inside the islands in the different collision regimes.

A. Density profile in the collisionless regime

First, the case with the large island is considered. Note that for the collisionless case ($\nu_{ii}^* = 0$), Jiang *et al.* have carried out a qualitative analysis on the radial profile of particle density inside the island separatrix.[21] Now, we present a quantitative analysis in this paper. Figures 2(a) and 2(c) show that ion density profiles across the O-points of two large islands (here, $w = 10w_b$) at HFS and LFS are different. The ion

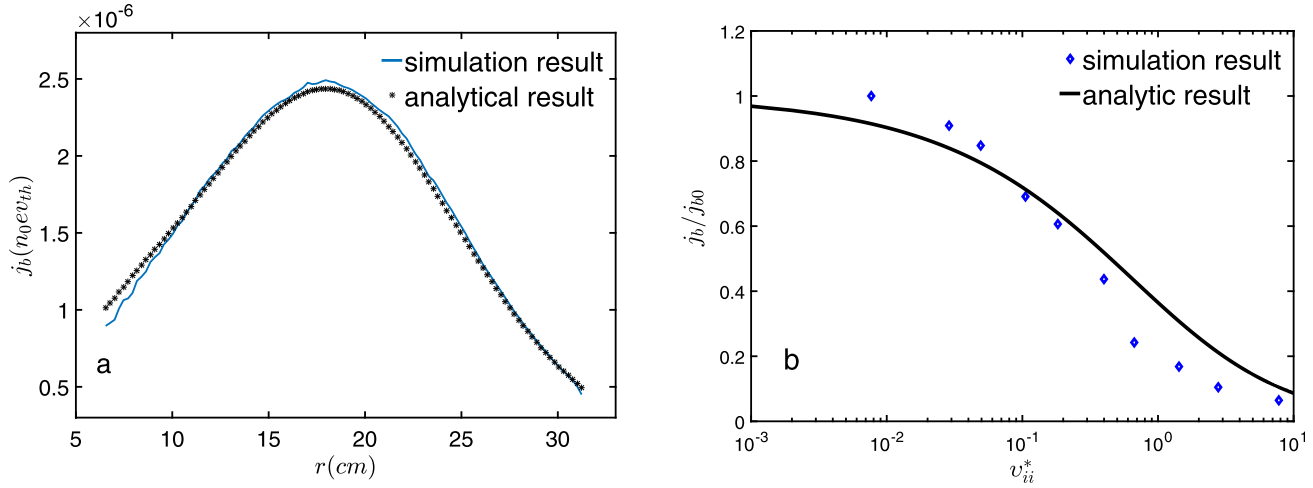

FIG. 1. (a) Radial profile of flux-surface-averaged ion bootstrap current (normalized by n_0ev_{th}) in the banana regime ($\upsilon_{ii}^* = 0.05$). (b) Saturated bootstrap current (normalized by j_{b0}) vs effective ion-ion collision frequency υ_{ii}^*.

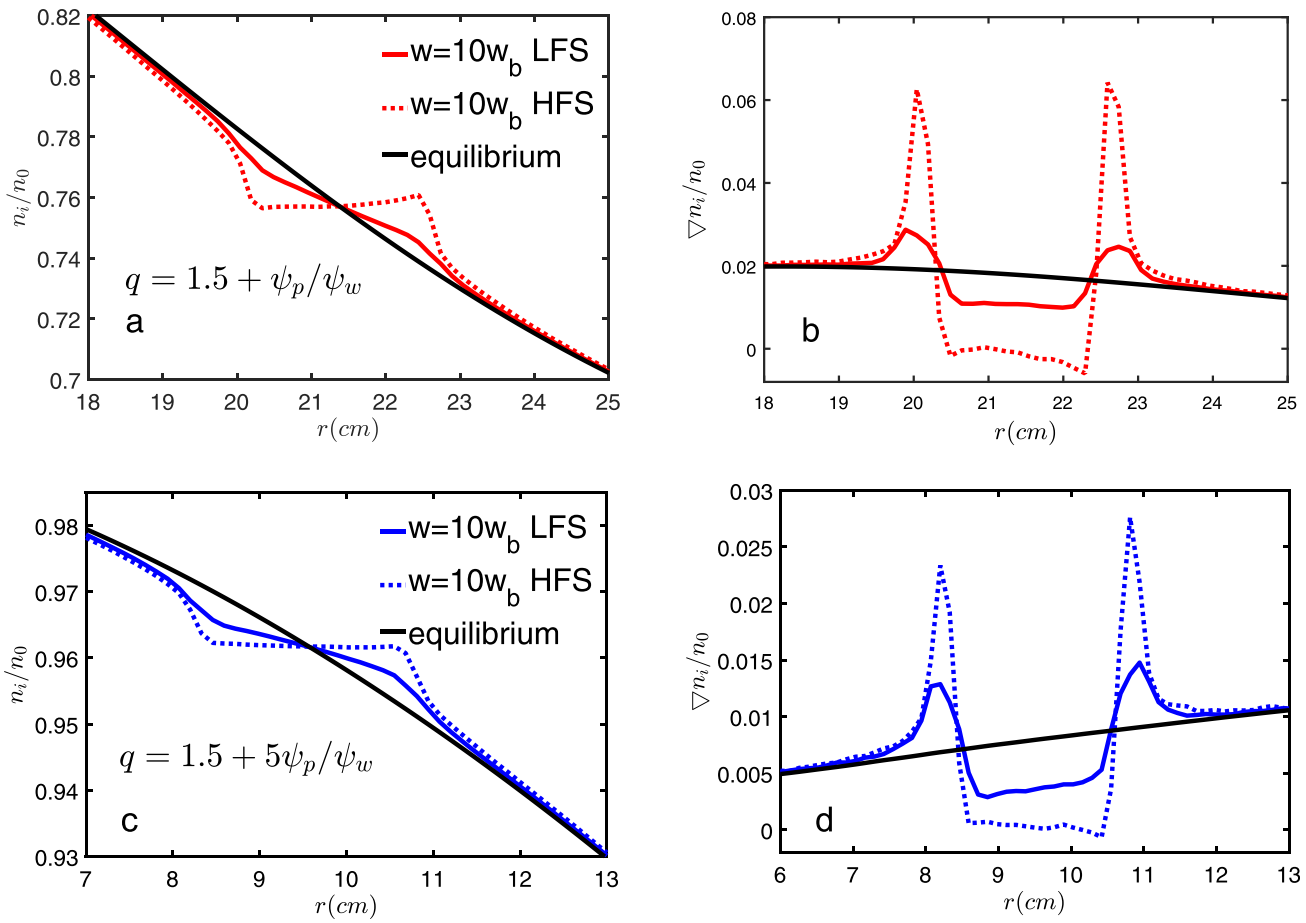

FIG. 2. Radial profiles of ion density and its gradient in the vicinity of the magnetic island with a width of $w = 10w_b$ in the collisionless regime. (a) and (b) $q = 1.5 + \psi_p/\psi_w$; (c) and (d) $q = 1.5 + 5\psi_p/\psi_w$.

density gradient mostly vanishes inside the island at HFS but partly survives at LFS. The difference may originate from the existence of trapped ions because they respond the magnetic island differently from the passing ions. As described above, the passing ions can move very fast along the perturbed field lines, and thus, their density distribution should be uniform on each island surface. Because most of the ions near $\theta = \pi$ are passing ones, the ion density profile across the O-point of the island at HFS is flattened. On the other hand, most of the trapped ions do not move in a circle on the island surfaces because their banana orbits are hardly affected by the magnetic island structure.[28] Their density gradient can almost remain as the equilibrium state. As a result, the density gradient can partly survive inside the island at LFS due to the existence of trapped ions. Furthermore, the flattening level of the ion density profile inside islands is evaluated. Figure 2(a) shows that the ion density profile is flattened roughly about 40% inside the island at LFS. For comparison, the corresponding analytical value is estimated: considering that in Fig. 2(a), $\varepsilon = 0.256$ is taken at the $q_s = 2/1$ surface and then the trapped fraction is $f_t \approx 0.6$, the ion density profile should have ~40% flattening inside the island at LFS, showing perfect agreement with the simulation. If $\varepsilon = 0.162$ is taken, Figs. 2(c) and 2(d) shows that the ion density profile can have ~50% flattening at $\theta = 0$ due to $f_t \approx 0.5$. For generality, the analytical values of the trapped fraction at several points (from the island center to $\Omega = 0$) inside the LFS island are compared with the simulation results of the survived density gradient ratio as plotted in Fig. 3, showing good agreement.

Second, the case with the small island is investigated. If the island width is comparable to the drift-orbit displacement width of the passing ions (i.e., $w = w_p = q_s\rho_i$), the profiles of the ion density gradient at both HFS and LFS are plotted in Fig. 4, in which the ion density gradient almost retains the equilibrium state in the vicinity of the LFS island and is largely recovered inside the HFS one. Such observations may be understood through the effects of both the banana orbit of trapped ions and the drift-orbit displacement of passing ions. It can be imagined that, near the separatrix, the drift orbits of some passing ions can partly locate inside the island and partly outside. These ions may not pass through the X-point and move in a circle around the whole island surfaces. These simulation results and the above physical imagination match well with the analytical theory[29] and previous simulations,[30] i.e., the ion orbit effects tend to recover the ion pressure gradient inside the islands.

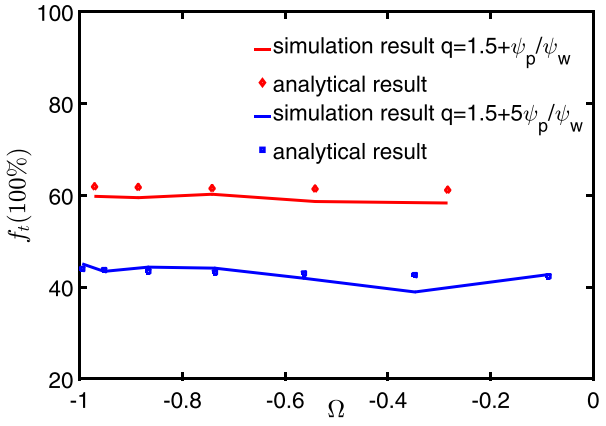

FIG. 3. Comparison of trapped ion fraction vs Ω at LFS for two cases with different q profiles. $\Omega = -1$ corresponds to the magnetic island center (O-point).

B. Density profile in collisional regimes

If the particle collision is considered, the physical understanding of the particle density profile recovery inside magnetic islands may be different. Here, for the magnetic island with a width of $w = 10w_b$, effective collision is evaluated in the banana regime ($\upsilon_{ii}^* = 0.05$). Figure 5 plots the time evolution of the density gradient in O-point regions of LFS and HFS islands separately. It can be seen that the density gradient inside both LFS and HFS islands decreases rapidly at the initial stage (i.e., before an ion-ion collisional period $t_1 = \tau_{ii} = 167R_0/v_{th}$). Such phenomena may be ascribed to the fact that the passing ions inside islands can move fast along the perturbed field lines after the island is formed and then flatten their density profile inside the islands. It can be imagined that the density profile of the passing ions with higher parallel velocity will be flattened more easily. Besides, Fig. 5 also shows that the decline of the density gradient inside the LFS island is slower than that inside the HFS island. This is because the trapped ions cannot move in a circle on the island surfaces.

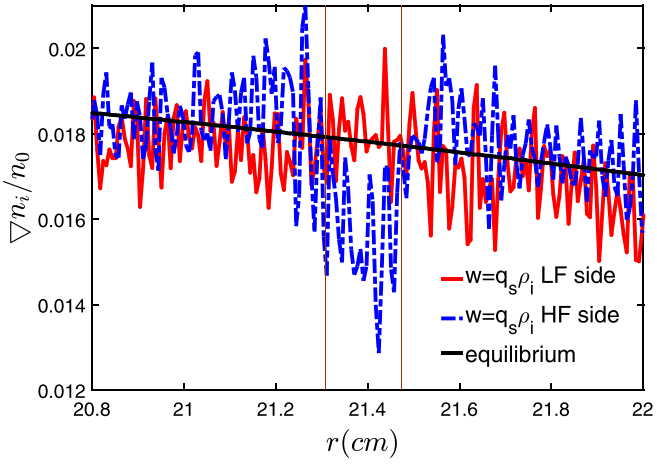

FIG. 4. Radial profiles of the ion density gradient in the vicinity of the magnetic island with $w = w_p = q_s\rho_i$ in the collisionless regime. Two vertical dashed lines label the island separatrix.

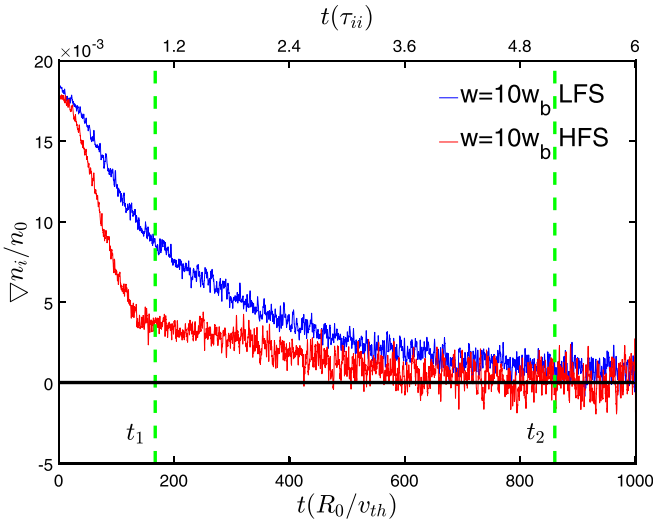

FIG. 5. Time evolution of the density gradient at O points (averaged over $\Delta\theta = 0.05\pi$) of LFS and HFS islands. The upper horizontal axis denotes the time normalized by the ion-ion collision period and the lower one normalized by R_0/v_{th}.

Furthermore, unlike that shown in Fig. 2(a), in which the density gradient inside the LFS island is at most 40% flattened, Fig. 5 shows that the density gradient inside the LFS island continuously decreases until it vanishes at $t_2 \approx 5\tau_{ii}$. The difference is due to the collision effect, which may greatly complicate the physical mechanism of the flattened density profile inside islands. It may be understood physically as follows: The density gradient of the trapped ions can remain before effective collisions take place, while that of passing ones has already dropped drastically as shown in Fig. 5. Note that large-angle collision can change the trapped or passing state of a charged particle in the confined magnetic field. If the trapped ions, whose whole banana orbits are located inside the islands, change into the passing ones via ion-ion collision, these originally trapped ions now can move fast along the closed field lines inside the island and then flatten their density profile. Meanwhile, the same number of passing ions can also become trapped via the collision. However, the density gradient of these originally passing ions has already been largely reduced inside islands before collision. As a result, their density gradient cannot be recovered even if these previously passing ions have become trapped ions. As more and more originally trapped ions change to the passing ones via collisions and then flatten their density profile, the density gradient of total ions finally vanishes inside the LFS island after several collision periods.

For the same problem above, Hornsby *et al.* have proposed that collisions scatter particles from the trapped to the passing domain and therefore reduce the radial gradient of the trapped population.[30] They have testified the proposal by simulations utilizing a code with a simplified model when small diffusion due to turbulence is considered.[19] In our simulations, similar results are achieved in the presence of all the drift orbit width effects, which are not included in that work.

Furthermore, note that the banana centers of some trapped ions are close to the island separatrix so that their banana orbits can be partly located inside and outside the island. In such a situation, the collision between trapped and passing ions cannot completely flatten the

density profile of these trapped ions near the separatrix inside the LFS island. Similarly, as introduced in Sec. III A, the density profile of the passing ions near the separatrix also cannot be completely flattened due to their drift-orbit displacement. Such physical dynamics are confirmed by GTC simulations, as shown in Figs. 6(a) and 6(b), in which the ion density gradient partly survives in a narrow layer with a width of $2w_b$ (or $2w_p$) near the separatrix of the LFS (or HFS) island, respectively.

On the other hand, Dong and Lin have pointed out that the electron density profile inside the magnetic island varies with different collision frequencies.[20] In our simulations, it can be noted that the ion density profile behaves in a similar way. For effective collision frequency in the plateau regime (here, $\upsilon_{ii}^* = 1.8$), the ion density gradient is partly recovered inside the island at both sides, as shown in Figs. 6(c) and 6(d). This suggests that even some passing ions cannot rapidly move in a circle around the whole closed surfaces inside the island before the collision so that they cannot reduce their density gradient inside islands.

Note that the temperature gradient also contributes to the bootstrap current besides the density gradient. The study on the ion temperature dynamics inside a magnetic island is just as important as the density. In fact, the FBW effects of trapped ions and displacement of passing ions could play a similar role in the ion temperature profile to the density. For example, Fig. 7 plots the ion temperature profile in a larger island with $w = 10w_b$, exhibiting alike characteristics to the density profile, as shown in Fig. 6(a). Here, $\upsilon_{ii}^* = 0.05$. However, this paper focuses on the ion density profile in the vicinity of the islands to compare with the results in Ref. 17. The detailed investigation on the temperature profile inside magnetic islands and in different collision regimes is left for future work.

IV. BOOTSTRAP CURRENT PROFILE VS MAGNETIC ISLAND WIDTH

We have mainly calculated the ion density profiles inside a magnetic island in different collision regimes in the Sec. III and provided a reasonable understanding of the underlying physical mechanism on the ion density gradient recovery inside the island. In the following, we will investigate the profiles of the ion density and bootstrap current in the vicinity of islands with different widths in the banana regime ($\upsilon_{ii}^* = 0.05$).

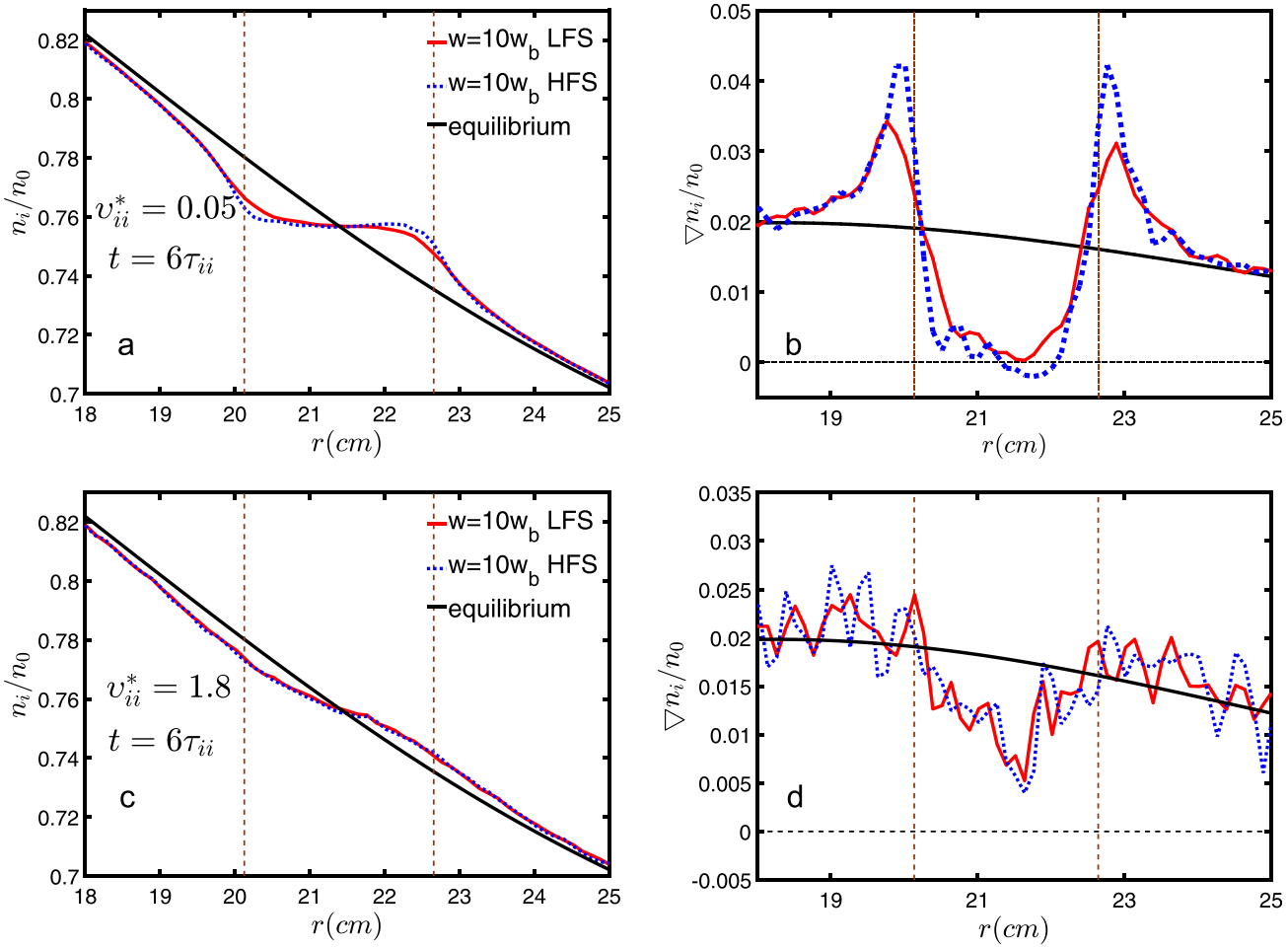

FIG. 6. Radial profiles of ion density and its gradient in the different collision regime. (a) and (b) $\upsilon_{ii}^* = 0.05$; (c) and (d) $\upsilon_{ii}^* = 1.8$. Vertical lines label the island separatrix.

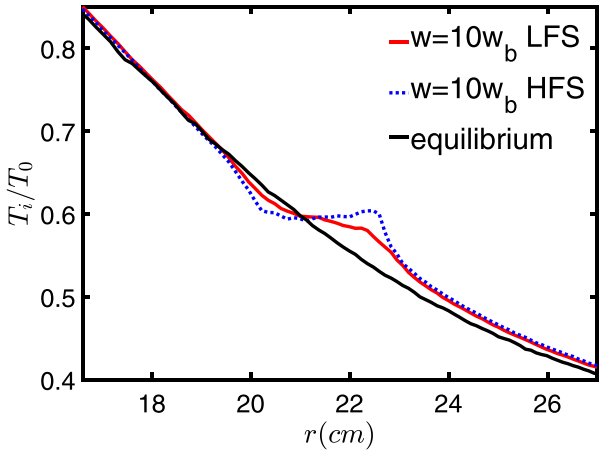

FIG. 7. Radial profile of ion temperature in the vicinity of large islands with $w = 10w_b$. $\upsilon_{ii}^* = 0.05$.

Here, GTC simulations are performed with different widths of magnetic islands taken as 1, 6, and 10 times of w_b. Figures 8(a) and 8(b) plot the corresponding ion density profiles at $t = 15\tau_{ii}$ after the island structure is formed. It can be seen from Fig. 8(a) that for the island width comparable to w_b, the density gradient can be completely recovered inside the islands at both sides. On the other hand, Fig. 8(b) shows that the density profile can be flattened inside the pretty large island. The difference in the density profiles inside the islands with different widths may be explained by the combination effects introduced in Sec. III: banana orbit of the trapped ion and the drift-orbit displacement of the passing one. Here, it should be pointed out that the results shown in Fig. 8(a) are different from those in Ref. 17, in which the recovery of the ion density gradient is not so obvious inside small islands.

As well known, the bootstrap current is proportional to the local density gradient if the temperature gradient is neglected. Therefore, the profile of the ion bootstrap current should match with the density. Such a relation is testified by GTC simulations, as shown in Fig. 9. Due to the recovery of the density gradient, there is almost no loss in the ion bootstrap current inside small islands at HFS and only a very little reduction at LFS, showing a perfect coincidence with the profiles of the density gradient in Fig. 8. It may suggest that the recovery of the ion bootstrap current inside small islands results mainly from the density gradient recovery. However, although the results in Fig. 9 are similar to those in Ref. 17, the understanding of the underlying physical mechanism of the ion bootstrap current recovery inside the small island is different. In that work, to explain the almost complete recovery of the ion bootstrap current inside the small island while the density profile still exhibits a significant residual flattening, it has been claimed that the trapped ions can feel the density gradient outside the island due to the overlap of the islands and banana orbits. The reduced ion bootstrap current contribution to the evolution of the small NTM magnetic islands has been simply expressed as[10]

$$\Delta_{bi,m} = \Delta_{bi}\frac{w^2}{w^2 + \alpha \cdot w_b^2}, \tag{5}$$

where Δ_{bi} is the ion bootstrap current driving term without the FBW effect. Here, numerical factor $\alpha = 7$, which is determined through simulations via the HAGIS code. In that work, the FBW effect has been assumed to play a dominant role in the recovery of the ion bootstrap current inside the islands and the reduction of the ion bootstrap current driving force. However, it has already been clarified that the role of the FBW effect in the reduction of $\Delta_{bi,m}$ is overestimated.[18] The recovery of the pressure gradient inside the island has been demonstrated to play a more important role than the FBW effect.

Furthermore, note that the recovery of the ion density gradient inside a magnetic island depends on not only the island width but also the ion collision frequency as presented above. Besides, it has also been commented that the recovery is further related to the island rotation.[31,32] The recovery caused by the island rotation can be comparable to the drift orbit width effect and the recovery level depends on both the frequency and the direction of the island rotation. All these results indicate that Eq. (5), or at least with a constant coefficient α, may not appropriately calculate the contribution of ion bootstrap current to the

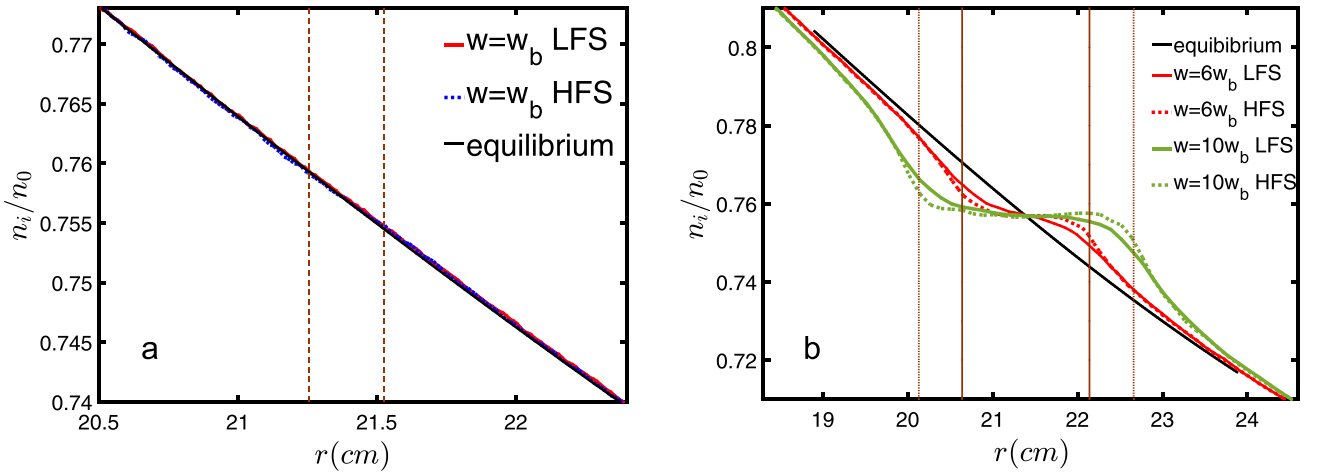

FIG. 8. Radial profile of ion density in the vicinity of islands for different widths $w = (1, 6, 10)w_b$. Vertical lines label the island separatrix.

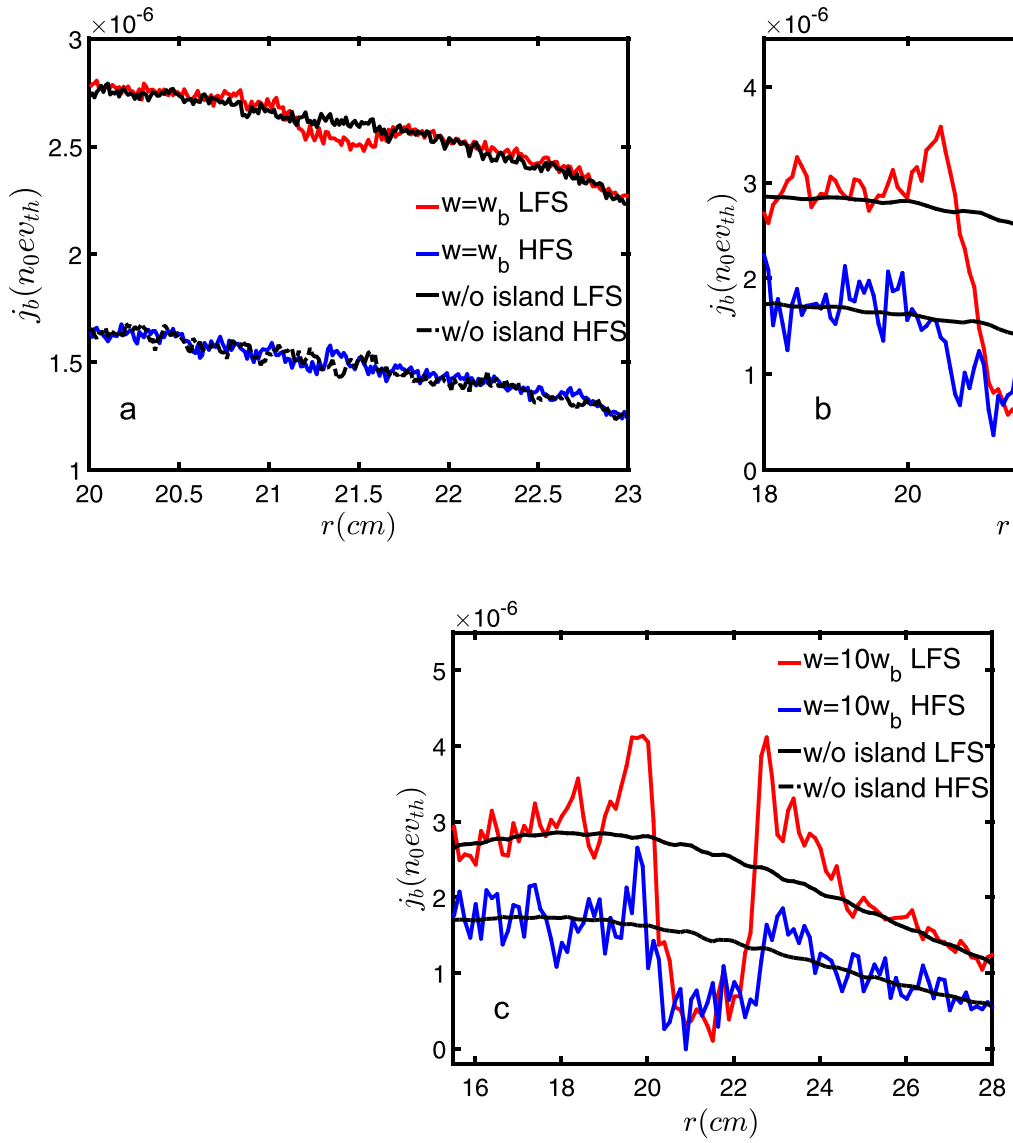

FIG. 9. Radial profile of ion bootstrap current in the vicinity of islands with widths (a) $w = w_b$; (b) $w = 6w_b$; and (c) $w = 10w_b$. The black solid and dashed-dotted lines denote the equilibrium ion bootstrap currents without the magnetic island.

evolution of the NTM island because α should be a function of the ion-ion collisionality and island rotation frequency. Hence, the direct application of Eq. (5) with constant α to evaluate the NTM island threshold in tokamak experiments may loss the basic guarantee in accuracy.

V. SUMMARY AND DISCUSSION

In this work, we have investigated the profiles of the ion density gradient and bootstrap current inside magnetic islands based on the first principles simulation via the GTC code. For simplicity, the contribution of the ion temperature gradient is neglected in evaluating the bootstrap current. Moreover, an island geometry with the $(m, n) = (2, 1)$ magnetic island due to the tearing mode is adopted and incorporated into the GTC code. Simulations are performed for different island widths and also in various collision regimes to clarify the underlying physical mechanism. The results suggest that the recovery of the pressure gradient inside the small island may play a more important role in the reduction of driving force of the ion bootstrap current in the evolution of the neoclassical tearing mode, rather than the so-called finite banana-orbit effect. Main achieved results are summarized as follows:

(a) In the collisionless regime, the ion density gradient mostly vanishes inside the HFS island but partly survives at LFS for larger magnetic islands. It is identified that the difference may originate from the existence of trapped ions because they respond to the magnetic island different from the passing ions. On the one

hand, the passing ions move very fast along the perturbed field lines so that their density distribution tends to be uniform on each island surface. On the other hand, the banana orbits of the trapped ions mainly located at LFS are hardly changed by the island structure, resulting in the ion density gradient partly remaining inside the LFS island.

(b) For the case with small islands in the collisionless regime, even the drift-orbit displacement of the passing ions can contribute to the recovery of the ion density gradient inside the HFS island.

(c) In the banana regime, the ion density gradient can be completely flattened inside large islands due to the collision between the trapped and passing ions, except in a thin layer near the separatrix with a width comparable to the banana orbit (LFS) or drift-orbit displacement (HFS). If the island width is comparable to the ion banana-orbit width, the density gradient can almost be recovered inside the island.

(d) In the plateau regime, the ion density gradient is partly recovered inside the islands at both HFS and LFS. It is suggested that even some passing ions cannot rapidly move in a circle around the whole closed surfaces inside the island before the collision so that they cannot reduce their density gradient inside islands.

(e) The recovery of the pressure gradient rather than the FBW effect inside the magnetic island has been demonstrated to play a more important role in the recovery of the ion bootstrap current inside the islands and the reduction of the ion bootstrap current driving force.

In fact, the underlying mechanisms about the recovery of the ion bootstrap current inside islands are rather complicated. Because the profiles of ion pressure in the vicinity of islands are related to not only the banana-orbit width but also the ion collision and island rotation and so on. To evaluate the NTM island threshold more accurately, the format of the bootstrap current term in the NTM evolution equation shown in Eq. (5) may need to be reconsidered. This work is beyond the scope of this paper and left for future investigation.

ACKNOWLEDGMENTS

This work was supported by the National Magnetic Confinement Fusion Science Program (Grant No: 2015GB110002). It was also partially supported by the National Key R&D Program of China under Grant Nos. 2017YFE0301200 and No. 2017YFE0301201 and National Natural Science Foundation of China under Grant Nos. 11775069 and 11875019.

REFERENCES

[1]P. H. Rutherford, Phys. Fluids **16**, 1903 (1973).
[2]A. I. Smolyakov, Plasma Phys. Controlled Fusion **35**, 657 (1993).
[3]H. R. Wilson, J. W. Connor, R. J. Hastie, and C. C. Hegna, Phys. Plasmas **3**, 248 (1996).
[4]R. Fitzpatrick, Phys. Plasmas **2**, 825 (1995).
[5]N. N. Gorelenkov, R. V. Rudny, Z. Chang, M. V. Gorelenkova, and L. E. Zakharov, Phys. Plasmas **3**, 3379 (1996).
[6]R. Carrera, R. D. Hazeltine, and M. Kotschenreuther, Phys Fluids **29**, 899 (1986).
[7]W. X. Qu and J. D. Callen, National Technical Information Service Document No. DE6008946, University of Wisconsin Plasma Report No. UWPR 85–5, 1985.
[8]Z. Chang, J. D. Callen, E. D. Fredrickson, R. V. Budny, C. C. Hegna, K. M. McGuire, M. C. Zarnstorff, and TFTR group, Phys. Rev. Lett. **74**, 4663 (1995).
[9]T. Oikawa, A. Isayama, T. Fujita, T. Suzuki, T. Tuda, and G. Kurita, Phys. Rev. Lett. **94**, 125003 (2005).
[10]E. Poli, A. G. Peeters, A. Bergmann, S. Günter, and S. D. Pinches, Phys. Rev. Lett. **88**, 075001 (2002).
[11]R. J. Buttery, T. C. Hender, D. F. Howell, R. J. La Haye, O. Sauter, D. Testa, and Contributors to the EFDA-JET Workprogramme, Nucl. Fusion **43**, 69 (2003).
[12]M. Maraschek, O. Sauter, S. Günter, H. Zohm, and ASDEX Upgrade Team, Plasma Phys. Controlled Fusion **45**, 1369 (2003).
[13]D. Zarzoso, F. J. Casson, W. A. Hornsby, E. Poli, and A. G. Peeters, Phys. Plasmas **22**, 022127 (2015).
[14]W. A. Hornsby, P. Migliano, R. Buchholz, S. Grosshauser, A. Weikl, D. Zarzoso, F. J. Casson, E. Poli, and A. G. Peeters, Plasma Phys. Controlled Fusion **57**, 054018 (2015).
[15]L. Bardóczi, T. L. Rhodes, T. A. Carter, A. B. Navarro, W. A. Peebles, F. Jenko, and G. McKee, Phys. Rev. Lett. **116**, 215001 (2016).
[16]A. B. Navarro, L. Bardóczi, T. A. Carter, F. Jenko, and T. L. Rhodes, Plasma Phys. Controlled Fusion **59**, 034004 (2017).
[17]E. Poli, A. G. Peeters, A. Bergmann, S. Günter, and S. D. Pinches, Plasma Phys. Controlled Fusion **45**, 71 (2003).
[18]H. Qu, F. Wang, A. Wang, X. Peng, and J. Li, Phys. Plasmas **25**, 054507 (2018).
[19]W. A. Hornsby, M. Siccinio, A. G. Peeters, E. Poli, A. P. Snodin, F. J. Casson, Y. Camenen, and G. Szepesi, Plasma Phys. Controlled Fusion **53**, 054008 (2011).
[20]G. Dong and Z. Lin, Nucl. Fusion **57**, 036009 (2017).
[21]P. Jiang, Z. Lin, I. Holod, and C. Xiao, Phys. Plasmas **21**, 122513 (2014).
[22]P. Jiang, Z. Lin, I. Holod, and C. Xiao, Plasma Sci. Technol. **18**, 126 (2016).
[23]Z. Lin, W. M. Tang, and W. W. Lee, Phys. Plasmas **2**, 2975 (1995).
[24]S. E. Parker and W. W. Lee, Phys. Fluids B **5**, 77 (1993).
[25]A. G. Peeters, Plasma Phys. Controlled Fusion **42**, B231 (2000).
[26]F. L. Hinton and R. D. Hazeltine, Rev. Mod. Phys. **48**, 239 (1976).
[27]Y. Wu and R. B. White, Phys. Fluids B **5**, 3291 (1993).
[28]E. Poli, M. Garc, H.-U. Fahrbach, S. Günter, and ASDEX Upgrade Team, Phys. Plamas **15**, 032501 (2008).
[29]H. Cai, D. Li, and J. Cao, Phys. Plasmas **22**, 102512 (2015).
[30]W. A. Hornsby, A. G. Peeters, A. P. Snodin, F. J. Casson, Y. Camenen, G. Szepesi, M. Siccinio, and E. Poli, Phys. Plasmas **17**, 092301 (2010).
[31]A. Bergmann, E. Poli, and A. G. Peeters, Phys. Plasmas **16**, 092507 (2009).
[32]D. Zarzoso, W. A. Horsby, E. Poli, F. J. Casson, A. G. Peeters, and S. Nasr, Nucl. Fusion **55**, 113018 (2015).